COMPARISON OF BIAXIAL MECHANICAL PROPERTIES OF CORONARY SINUS TISSUES FROM PORCINE, OVINE AND AGED HUMAN SPECIES

Thuy Pham and **Wei Sun**
Tissue Mechanics Lab Biomedical Engineering Program and Mechanical Engineering Department University of Connecticut, Storrs, CT 06269

Abstract

Due to its proximity to the mitral valve, the coronary sinus (CS) vessel serves as a conduit for the deployment and implantation of the percutaneous transvenous mitral annuloplasty (PTMA) devices that can potentially reduce the mitral regurgitation. Because CS vessel is a venous tissue and seldom diseased, its mechanical properties have not been well studied. In this study, we performed the multi-axial mechanical test and histological analysis to characterize the mechanical and structural properties of the aged human, porcine and ovine CS tissues. The results showed that the aged human CS tissues exhibited much stiffer and highly anisotropic behaviors compared to the porcine and ovine. Both of the porcine and ovine CS vessel walls were thicker and mainly composed of striated muscle fibers (SMF), whereas the thinner aged human CS had higher collagen, lesser SMF, and more fragmented elastin fibers, which are possibly due to the aging effects. We also observed that the anatomical features of porcine CS vessel might be not suitable for the PTMA deployment. These differences between animal and human models raise questions for the validity of using animal models to investigate the biomechanics involved in the PTMA intervention. Therefore, caution must be taken in future studies of PTMA stents using animal models.

Keywords

coronary sinus; mitral valve regurgitation; percutaneous intervention; biomechanics tissue properties

1. INTRODUCTION

Functional mitral regurgitation (MR) is a consequence of left ventricular dysfunction that may occur after ischemic heart disease and often has poor prognosis. Left ventricular dilation in functional MR leads to mitral annulus enlargement and incomplete mitral leaflet apposition, though the valve leaflets remain normal in structure and function. The current treatments for severe functional MR are surgical repair and replacement of the mitral valve. However, the technique carries a high mortality rate (Ellis et al. 1965, Gillinov et al. 2001,

For correspondence: Wei Sun, Ph.D. 207 Bronwell Building University of Connecticut Storrs, CT 06269-3139 Phone: (860) 486-0369 Fax: (860) 486-5088 weisun@engr.uconn.edu.

Jamieson et al. 1989) and is not suitable for patients with comorbidities or advanced age (Cohn et al. 1995, Grossi et al. 2001, Hausmann et al. 1999).

Recently, a new non-surgical intervention method, percutaneous transvenous mitral annuloplasty (PTMA), is being investigated as an endovascular alternative to the highly invasive open-heart surgery. The technique utilizes the location of the coronary sinus (CS) vein, which courses along the atrioventricular groove and is adjacent to the posterior mitral annulus, to embed a PTMA device that can reduce the annular diameter and thus MR. Several PTMA devices, including Carillon (Cardiac Dimensions Inc., NE Kirkland, WA,USA), Viacor (Viacor Inc., Wilmington, MA, USA), and Monarc (Edwards Lifesciences Corp., Irvine, CA, USA), have been evaluated in animal models (Byrne 2004, Daimon et al. 2005, Kaye et al. 2003, Liddicoat et al. 2003, Maniu et al. 2004). The immediate short-term reduction of the annulus diameter in animal trials has led to several first-in-human clinical studies (Duffy et al. 2006, Hoppe et al. 2009, Siminiak et al. 2007, Siminiak et al. 2009, Webb et al. 2006). Moderate to significant reductions in MR were observed in these human studies. However, severe adverse events associated with the procedure were reported, such as compression of the coronary arteries (e.g. the left circumflex artery), perforation of vessel branches, unsuccessful device implantation due to the highly variable geometries of the coronary venous anatomy or the lack of appropriately-sized devices, device migration resulted from the reduction of anchoring tension and device fracture. Some of these issues may be improved by a detailed anatomical assessment of the CS and its tributaries prior to the procedure using coronary angiography, multidetector computed tomography and echocardiography. Device dysfunctions involving device migration and fracture, however, are mainly associated with the biomechanical interaction between host tissues and the device that has yet to be well studied in the literature.

Quantification of the mechanical properties of the CS vessel is critical for estimating the tissue-implant biomechanical interaction and for understanding device failure mechanisms. Although the anatomical studies of the CS have been well reported (Barceló et al. 2004, Chauvin et al. 2000, Loukas et al. 2009), there is a dearth of study on the mechanical properties of the tissue. Recently, Pham and Sun (Pham and Sun 2010) reported the diameter-pressure relation of porcine CS from a vessel inflation experiment. There are two limitations in the paper: 1) the experiment was conducted under relatively simple pressure inflation loading conditions, and 2) only the porcine CS was examined. Due to complex tissue-device interactions, quantification of tissue behaviors under multi-axial loading conditions may be needed. Moreover, a study of CS tissue properties from different species (i.e., porcine, ovine and human) may be helpful in understanding the outcomes among animal trials and human studies, and establishing a proper animal model to evaluate the device efficacy.

In this study, we studied the mechanical properties of the CS wall from porcine, ovine and human models. The human cadaver CS tissues were selected from an age group of 86.5 ± 9.7 years old. The CS tissues were subjected to multi-protocol biaxial tests and characterized by the Fung-type elastic model. Histological analysis was also performed to compare the difference in tissue microstructure among porcine, ovine and aged human CS tissues.

2. MATERIALS AND METHODS

2.1 Materials

Human cadaver hearts were obtained from Cardinal Biologicals, Inc. (Tyler, TX; n = 2) and National Disease Research Interchange (NDRI, Philadelphia, PA; n = 8). The use of human tissues was approved by the Institutional Review Board at the University of Connecticut. The hearts were fresh frozen within a post-mortem recovery interval (15.32 ± 6.51 hours)

and remained frozen until delivery on the next day. All hearts were stored in a -80°C freezer and were taken out individually for testing within 3 months. Porcine hearts (n = 10, 6 - 9 months old with a weight range of 418.60 ± 71.81 g) from the Animal Technologies, Inc. (Tyler, TX) and sheep hearts (n = 10, 1 year old, 280.08 ± 28.17 g) from the Brother Quality, Inc. (Stafford Springs, CT) were obtained fresh and stored in a -80°C freezer until testing within 2 weeks.

Following the two-stage slow thawing method proposed by Bia et al. to void tissue damages (Bia et al. 2006), each heart was held at room temperature (20°C) for 30 minutes and then submerged in a 37°C water bath until totally defrosted. The entire CS vessel could be removed from the heart because only the anterior section of the vessel is partially embedded in the myocardium, as shown in Fig. 1. After carefully procuring the vessel and removing the excess tissues (e.g. fat and loose connective tissues), a square specimen, about 15 mm in length, and at a region near the CS ostium end (or the proximal section), was excised for testing, see Fig. 1. The tissue thickness was measured at six regions with a thickness gauge (Mitutoyo, Model 7301) and the average value was recorded. Four small graphite markers were placed at the center on the inner surface of the posterior (i.e., myocardium-free) section of the CS vessel to demarcate a small quadrilateral for strain calculation.

2.2 Planar biaxial mechanical testing

Details on planar biaxial mechanical testing techniques and methods of analysis adopted in this study can be found in Sacks and Sun 2003 (Sacks and Sun 2003). Briefly, all specimens were mounted in a trampoline fashion, and the vessel circumferential and longitudinal directions were aligned with the primary axes of the biaxial test fixtures. Human tissue samples were tested in a Ca^{2+}-free phosphate buffered saline (PBS) solution at 37°C. Due to their young age and relatively high muscle content, animal tissue samples were tested in a Ca^{2+}-free and glucose-free Tyrode solution (mM: NaCl 136.9, KCl 2.7, MgCl2 1.05, NaHCO3 11.9, NaHPO4 0.47, EGTA 2.0, and 0.1M papaverine) at 37°C. Using Ca^{2+}-free solution is to minimize the active contraction of muscle fibers in order to obtain the passive mechanical properties of the CS vessel. Adding EGTA, a chelating agent with a high affinity for Ca^{2+}, would actively remove the intracellular Ca^{2+} concentration. The similar protocols have been used in studies of passive blood vessel mechanical properties (Alastrué et al. 2008, Carboni et al. 2007, Desch and Weizsäcker 2007, García et al. 2011, Schulze-Bauer et al. 2003). As reported by Tritthart *et al.* (Tritthart et al. 1973), exposing Ca^{2+}-free solution several times in succession could have a comparable result as to the EDTA-containing solution. A stress-controlled test protocol was utilized (Sun et al. 2003), wherein the ratio of the normal Lagrangian stress components $T_{11} : T_{22}$ was kept constant with $T_{12} = T_{21} = 0$. Maximum load was applied without causing tears at the edges of the specimens. Preconditioning was performed to minimize tissue hysteresis. Each tissue specimen was preconditioned for at least 40 continuous cycles with $T_{11} : T_{22} = 1 : 1$. Seven successive protocols were performed using ratios $T_{11} : T_{22} = 1 : 0.3, 1 : 0.5, 1 : 0.75, 1 : 1, 0.75 : 1, 0.5 : 1$, and $0.3 : 1$. This range was chosen for extensive coverage of the in-plane strain state (Sacks and Sun 2003). All specimens were cryopreserved (Bia et al. 2006) after biaxial testing and stored at -80°C.

2.3 Histology

The structural constituents of the CS vessel, primarily elastin, collagen, and muscle fibers, were analyzed across the thickness. After thawing and removing the cryoprotectant agent following a protocol proposed by Bia et al. (Bia et al. 2006), tissue specimens were fixed in 10% formalin for 24 hours. Each sample was dehydrated through a process of varied alcohol concentrations, embedded in paraffin, and sectioned at 5 μm in thickness. Samples were then mounted on microscope slides and dried. After deparaffinization, slides were then stained

with Verhoeff Van-Gieson (VVG). Elastic fibers could be visualized as black strands, collagen fibers as red, muscle fibers as a duller red or light brown color. Histological images were obtained from an Olympus U-TVO.5xC digital camera coupled to an Olympus BX40 light microscope.

2.4 Constitutive Modeling

The coronary sinus tissue was assumed to be homogeneous, non-linear hyperelastic and anisotropic. Therefore, the Fung-type elastic model (Fung 1993) was used to characterize the biaxial experimental data. The in-plane second Piola-Kirchhoff stresses, *S*, were derived from a strain energy function *W*,

$$S_{ij} = \frac{\partial W}{\partial E_{ij}}$$

(1)

where E_{ij} is the Green-Lagrange strain tensor and *W* is expressed as:

$$W = \frac{c}{2}\left(e^Q - 1\right)$$

(2)

and *Q* as:

$$Q = A_1 E_{11}^2 + A_2 E_{22}^2 + 2A_3 E_{11} E_{22} + A_4 E_{12}^2 + 2A_5 E_{11} E_{12} + 2A_6 E_{22} E_{12}$$

(3)

with *c* and A_{1-6} are material parameters.

The constitutive model was fit to the seven stress-controlled protocols for each individual specimen to obtain the material parameters. The goodness of the fit was determined by the R-square value based on the nonlinear regression Levenberg-Marquardt algorithm in SYSTAT 10 (Systat Software Inc., Chicago, IL). Each parameter set was tested for convexity using the method in Sun and Sacks 2005 (Sun and Sacks 2005). Variation of the parameters is presented in terms of the standard deviation.

2.5 Data Analysis

The mechanical properties of the human CS were quantified and compared to those of ovine and porcine CS tissues. The tissue stiffness was investigated by means of the secant modulus at a low stress value of 15 kPa and a high stress value of 50 kPa. One of the human CS specimens (Specimen 2) has a maximum testable stress below 35 kPa in both the circumferential and longitudinal directions, therefore, was omitted in the stiffness analysis at 50 kPa.

To quantify the degree of anisotropy (DA) among the specimens, the ratio of circumferential to longitudinal strains at 15 and 50 kPa stresses from the equibiaxial protocol ($T_{11} : T_{22} = 1 : 1$) was used. Thus, $DA = E_{22} : E_{11}$. A DA value of 1 indicates an isotropic tissue response, whereas other values represent various degrees of anisotropy. In addition, the relationship between age and 1) thickness, 2) stiffness, and 3) maximum equibiaxial strain in human specimens were also investigated.

2.6 Statistical Analysis

Differences between means were determined using the analysis of variance (ANOVA) test followed by the Holm-Sidak test and the Dunn's Method test for pair-wise multiple

comparisons. The Independent two-sample t-test was used to determine significant differences in anisotropy. Non-parametric tests, including the Wilcoxon signed-rank test and Mann-Whitney rank sum test, were used for non-normal distributed sample groups. Correlation was determined using the Pearson's correlation coefficient (r), and p-values were calculated based on the aforementioned statistical tests. All values of measurement are presented as a mean ± standard deviation. A probability value less than 0.05 was considered statistical significant, with high significance indicated by $p < 0.001$. Statistical analyses were performed using SigmaPlot (V11.0, Systat Software Inc., San Jose, CA).

3. RESULTS

3.1 Patient characteristics and specimen thickness

Table 1 lists characteristics of human hearts investigated in this study, including patient age, gender, cause of death, primary disease, and risk factors. The thickness of all CS specimens was determined. Human (0.74 ± 0.16 mm) and ovine (0.78 ± 0.12) were not significantly different ($p = 0.537$). However, porcine CS (1.24 ± 0.18) was significantly thicker than human ($p < 0.001$) and ovine ($p < 0.001$).

3.2 Biaxial mechanical behavior

Individual equibiaxial responses for ten human CS vessels are plotted in Fig. 2-A&B. There was a large variation in mechanical responses in both circumferential and longitudinal directions within the human samples, particularly the circumferential response which varied the most from a minimum strain of 0.18 in Spec 6 to a maximum of 0.45 in Spec 7. At low stress, the circumferential direction was very extensible, while the longitudinal direction stiffened more rapidly at low strain. At high stress above 20 kPa, the tissue response in both directions exceeded the typical "toe" region and exhibited rapid stiffening.

To compare the stress-strain responses of human, ovine and porcine specimens, mean response curves for each species are plotted in Fig. 3. All tissues exhibited the nonlinear stress-strain behavior of a typical blood vessel. However, a more gradual transition from low to high stiffness regions was observed in ovine and porcine, while human CS had a more pronounced rapid stiffening effect at the transitional region in both directions.

Differences in tissue properties among the species were examined by means of the secant moduli at stress levels of 15 and 50 kPa. In Fig. 4, a statistically significant difference was found between human and ovine ($p < 0.001$ at 15 kPa and $p = 0.001$ at 50 kPa) and between human and porcine ($p = 0.002$ at 15 kPa and $p = 0.003$ at 50 kPa) in the longitudinal direction. Ovine and porcine tissues did not differ at either stress level ($p = 0.449$ at 15 kPa and $p = 0.437$ at 50 kPa). For the circumferential response, only human and porcine tissues were significantly different at 50kPa, with $p = 0.024$.

The DA value by means of the strain ratio at a stress of 50 kPa was determined. The anisotropy of human tissues (0.59 ± 0.26) was greater than those of porcine (0.78 ± 0.15) and ovine (1.02 ± 0.37). Ovine tissue exhibited a nearly isotropic response, which can be seen in Fig. 3. To further analyze the tissue anisotropy, a paired-t test was used to quantify the association between the two directions of each species. Human and porcine exhibited a statistically significant anisotropy with $p = 0.004$ and $p = 0.002$, respectively, while ovine tissues did not show anisotropy, $p = 0.618$.

Statistical analysis did not reveal any correlation between age and thickness, stiffness, and maximum strain in human specimens. Though there was not enough data to group the results based on medical conditions, equibiaxial data did show that stress-strain curves of three hypertensive patients were shifted to the left of the data range (Fig. 2).

3.3 Constitutive Modeling

The constitutive parameters for each species are summarized in Table 2. The Fung-type elastic model was able to capture the CS planar biaxial mechanical behavior well with the high R-square (R^2) value of 0.95 ± 0.03 for human, 0.93 ± 0.09 for porcine and 0.93 ± 0.05 for ovine. Representative curve fitting plots of human, ovine and porcine CS are shown in Fig.5.

3.4 Histology

Differences in the microstructure between human, ovine and porcine specimens can be seen in Fig. 6. In Fig. 6, the circumferential histology images of CS posterior section of each species showed differences in the content of striated muscle fibers (SMFs) and elastic constituents. The intima layer of aged human CS tissues was composed of a highly dense network of collagen fibers which intertwined with longitudinal elastin fibers. It was prominently thicker than those of younger ovine and porcine tissues. The decrease in wall media in human tissues was accompanied by a significant decrease in the SMFs and a noticeable increase in collagen fibers. Elastin were found to be abundant in both the internal elastic lamina and the media but organized in multiple fragmented layers. In contrast, elastin fibers as well as collagen were less developed in younger ovine and porcine tissues.

Studies on the CS anatomy reported a continuous cuff of striated muscle surrounding the external wall of the CS vessel (Barceló et al. 2004, Chauvin et al. 2000). Similar structure was observed in all specimens. However, in human CS tissues, the striated muscle cuff is scarcely distributed around the posterior wall, that is the free-wall region of the CS. In contrast, the muscle cuff covered the posterior sections and accounted for the majority of the wall thickness in both ovine and porcine tissues. The anterior section of the CS wall for human, ovine, and porcine tissues was composed mainly of the striated muscle fibers with dispersed elastin and collagen fibers.

4. DISCUSSION

4.1 Anatomical differences

Several anatomical differences of the coronary venous vasculature between human, porcine and ovine species were observed. First, the oblique vein of Marshal (OVM) of the left atrium is found in human while the left precaval vein (LPV) is seen in both porcine and ovine, see Fig. 7. Both the OVM and LPV are remnants of the left superior vena cava. The LPV is completely patent and its diameter is larger than that of the OVM, but they both have the same function, which is to drain blood into the coronary sinus. The porcine LPV is found to be the largest and appears to be a continuation of the CS. The larger LPV, in some cases, resulted in a reduction of CS length and a wider junction of the LPV, GCV and CS. This could possibly prompt stent slippage due to lack of anchoring if positioned near the junction. Second, the GCV was observed to be narrowest in porcine, and the ovine GCV was smaller but similar in size to the human GCV. For the distal anchor of the PTMA device to be deployed, the GCV diameter needs to be equal or larger than 3 mm (Harnek et al. 2010). The porcine GCV appeared to be smaller than 3 mm in diameter and might not be suitable for the distal anchor deployment. Lastly, a high variation in the location of the left circumflex artery (LCX) was observed in all species, suggesting a careful imaging assessment prior to the procedure is necessary to reduce LCX perforation and impingement in the coronary flow in all species.

4.2 Mechanical properties and implications of PTMA intervention

Our results showed that the excised human CS stress-strain relationship is non-linear and anisotropic with the circumferential direction being more compliant. When comparing with

ovine and porcine CS tissues, human tissues were found to be stiffer and highly anisotropic. High stiffness of human CS tissues might be accounted for by the advanced age of the patients selected in this study (86.5 ± 9.7 years). Tissue stiffness has been shown to increase with age due to the degeneration and fragmentation of elastin fibers (Kohn 1977) and an increase of collagen content (Laurent et al. 2005, Pezet et al. 2009) which were observed in our human CS tissues. Therefore, it is possible that the mechanical properties of older porcine and ovine CS tissues more closely resemble those of an aged human, although this has not been assessed.

Animal models were first tested to evaluate the feasibility of the PTMA devices for the treatment of MR. Previous studies using ovine models demonstrated the feasibility of PTMA devices in reducing MR. However, for the human trials of three PTMA devices reported in 2006 and 2007, the results were suboptimal. Specifically, Webb et al. (Webb et al. 2006) reported fracture of the device bridge element in three of four patients implanted with a permanent Monarc PTMA device. Duffy et al. (Duffy et al. 2006) observed that the distal anchor of a Carillon PTMA device did not hold tension during device traction in two of five temporarily implanted patients. Dubreuil et al. (Dubreuil et al. 2007) reported temporary placements of a Viacor PTMA device in patients with an ischemic MR and MA dilation. They found that the MA diameter after the device implantation remained large compared to the surgical annuloplasty results. A more recent study in 2010 on the second generation Monarc PTMA device reported a reduction in MR by ≥ 1 grade at 12 months in 50% of 22 implanted patients (Harnek et al. 2010). Unsuccessful implantations were associated with the lack of appropriately-sized devices ($n = 13$), inaccurate device positioning resulting in no MR reduction ($n = 4$), device migration ($n = 1$) and fracture of the proximal anchor ($n = 4$). Thus, the success of PTMA animal trials was not reflected in human trials. Even though doubts always exist regarding the validity of animal models and their applicability to humans, there is clearly a lack of scientific evidence and engineering quantification of the discrepancy between animal and human trials.

In this study, we observed substantial differences in material properties between the animal and human CS, where the animal CS tissues were more compliant and deformable than the human ones. This indicated that the biomechanical environment in which the PTMA device is embedded was different in animals and humans. Therefore, the PTMA device might function well in animal models due to a relatively low tissue-stent interaction force. In contrast, under the stiffer mechanical environment in humans, the PTMA device may experience a higher interaction force which could possibly affect its durability. This observation underscores the importance of having an appropriate animal model for evaluating device function for its ultimate use in human.

4.3 Limitations and future study

The age range for the majority of MR patients is 60-70 years. In this study, our patient group is 87 ± 10 years old. The material properties of soft tissues were known to be stiffer with age and diseased cardiac tissues are age-related. However, in this study, we did not study the influence of age on the human CS tissues and only compared the available aged human group to animal types. In addition, due to limited access to fresh human tissues, in this study, we used fresh frozen human tissues. To facilitate the comparison of human, porcine and ovine tissues, we also froze fresh porcine and ovine tissues at -80°C prior to biaxial mechanical testing. Thus, by utilizing a similar freezing protocol for all of our samples, we could avoid inconsistency in tissue storage. Nonetheless, the fact that we do not have fresh human tissue is a limitation of this study.

Our histological analysis showed that CS is non-homogenous and composed of layers of constituents (elastin, collagen, and striated myocardial fibers). In this study, the CS was

modeled as a single-layer homogenous structure. A multiple layered material model incorporating structure-motivated phenomenon might provide a more accurate estimate of layer-specific material properties (Holzapfel et al. 2005). Other imaging methodologies such as scanning electron and two-photon laser scanning confocal microscopy might be helpful for collagen and fiber structural analysis (e.g., the fiber diameter and undulation period), to further correlate the structural findings with the mechanical properties of the vessel. Moreover, PTMA devices interact with the CS wall as well as the surrounding tissues, i.e., the mitral annulus, leaflets, chordae tendineae and the adjacent myocardium. To fully evaluate the PTMA device function, the mechanical properties of these interposed tissues, besides the CS wall, need to be quantified as well. Lastly, the sample size for each species in this study was relatively small; a larger sample size would provide more conclusive results.

5. CONCLUSIONS

We observed a discrepancy in mechanical and microstructural properties of CS vessels in aged human, ovine and porcine species. Overall, the human CS vessels were stiffer in both the circumferential and longitudinal directions than the ovine and porcine CS vessels. Higher collagen, lesser SMF, and fragmented elastin fibers found in human CS tissues demonstrated the effects of aging. This study also showed that the mechanical properties of CS tissues varied largely among patients. PTMA device studies involving animal models should be evaluated carefully given the distinguishable mechanical and structural differences between aged human, ovine, and porcine CS vessels obtained in this study.

Acknowledgments

REFERENCES

Alastrué V, Peña E, Martínez MA, Doblaré M. Experimental study and constitutive modelling of the passive mechanical properties of the ovine infrarenal vena cava tissue. Journal of Biomechanics. 2008; 41:3038–3045. [PubMed: 18789443]

Barceló A, Fuente LMDl, Stertzer SH. Anatomic And Histologic Review of The Coronary Sinus. Int. J. Morphol. 2004; 22:331–338.

Bia D, et al. Cryopreservation procedure does not modify human carotid homografts mechanical properties: an isobaric and dynamic analysis. Cell and Tissue Banking. 2006; 7:183–194. [PubMed: 16933040]

Byrne MJ, Kaye DM, Mathis M, Reuter DG, Alferness CA, Power JM. Percutaneous mitral annular reduction provides continued benefit in an ovine model of dilated cardiomyopathy. Circulation. 2004; 110:3080–3092.

Carboni M, Desch GW, Weizsäcker HW. Passive mechanical properties of porcine left circumflex artery and its mathematical description. Medical Engineering & Physics. 2007; 29:8–16. [PubMed: 16497534]

Chauvin M, Shah DC, Haïssaguerre M, Marcellin L, Brechenmacher C. The Anatomic Basis of Connections Between the Coronary Sinus Musculature and the Left Atrium in Humans. Circulation. 2000; 101:647–652. [PubMed: 10673257]

Cohn LH, Rizzo RJ, Adams DH, Couper GS, Sullivan TE, Collins JJ Jr, Aranki SF. The effect of pathophysiology on the surgical treatment of ischemic mitral regurgitation: operative and late risks of repair versus replacement. European Journal of Cardio-Thoracic Surgery. 1995; 9:568–574. [PubMed: 8562102]

Daimon M, Shiota T, Gillinov AM, Hayase M, Ruel M, Cohn WE, Blacker SJ, Liddicoat JR. Percutaneous mitral valve repair for chronic ischemic mitral regurgitation: A real-time three-dimensional echocardiographic study in an ovine model. Circulation. 2005; 111:2183–2189. [PubMed: 15851597]

Desch GW, Weizsäcker HW. A model for passive elastic properties of rat vena cava. Journal of Biomechanics. 2007; 40:3130–3145. [PubMed: 17512529]

Dubreuil O, Basmadjian A, Ducharme A, Thibault B, Crepeau J, Lam JYT, Bilodeau L. Percutaneous mitral valve annuloplasty for ischemic mitral regurgitation: First in man experience with a temporary implant. Catheterization and Cardiovascular Interventions. 2007; 69:1053–1061. [PubMed: 17525965]

Duffy SJ, Federman J, Farrington C, Reuter DG, Richardson M, Kaye DM. Feasibility and short-term efficacy of percutaneous mitral annular reduction for the therapy of functional mitral regurgitation in patients with heart failure. Catheter Cardiovasc Interv. 2006; 68:205–210. [PubMed: 16817176]

Ellis FHJ, Callahan JA, McGoon DC, Kirklin JW. Results of open operation for acquired mitral valve disease. N Engl J Med. 1965; 272:869–874. [PubMed: 14272755]

Fung, YC. Biomechanics: Mechanical Properties of Living Tissues. Springer Verlag; New York: 1993.

García A, Peña E, Laborda A, Lostalé F, De Gregorio MA, Doblaré M, Martínez MA. Experimental study and constitutive modelling of the passive mechanical properties of the porcine carotid artery and its relation to histological analysis: Implications in animal cardiovascular device trials. Medical Engineering and Physics. 2011; 33:665–676. [PubMed: 21371929]

Gillinov AM, Wierup PN, Blackstone EH, Bishay ES, Cosgrove DM, White J, Lytle BW, McCarthy PM. Is repair preferable to replacement for ischemic mitral regurgitation? J Thorac Cardiovasc Surg. 2001; 122:1125–1141. [PubMed: 11726887]

Grossi EA, et al. Ischemic mitral valve reconstruction and replacement: comparison of long-term survival and complications. J Thorac Cardiovasc Surg. 2001; 122:1107–1124. [PubMed: 11726886]

Harnek J, Webb JG, Kuck KH, Tschope C, Vahanian A, Buller CE, James SK, Tiefenbacher CP, Stone GW. Transcatheter implantation of the MONARC coronary sinus device for mitral regurgitation. JACC: Cardiovascular Interventions. 2010; 4:115–122. [PubMed: 21251638]

Hausmann H, Siniawski H, Hetzer R. Mitral valve reconstruction and replacement for ischemic mitral insufficiency: Seven years' follow up. Journal of Heart Valve Disease. 1999; 8:536–542. [PubMed: 10517396]

Holzapfel GA, Sommer G, Gasser CT, Regitnig P. Determination of layer-specific mechanical properties of human coronary arteries with nonatherosclerotic intimal thickening and related constitutive modeling. Am J Physiol Heart Circ Physiol. 2005; 289:2048–2058.

Hoppe UC, Brandt MC, Degen H, Dodos F, Schneider T, Stoepel C, Kroener A, Haude M. Percutaneous Mitral Annuloplasty Device Leaves Free Access to Cardiac Veins for Resynchronization Therapy. Catheterization and Cardiovascular Interventions. 2009; 74

Jamieson WRE, Burr LH, Munro AI, Miyagishima RT, Gerein AN. Caridac valve replacement in the elderly: Clinical performance of biological prostheses. Annals of Thoracic Surgery. 1989; 48:173–185. [PubMed: 2764609]

Kaye D, Byrne M, Alferness C, Power J. Feasibility and shortterm efficacy of percutaneous mitral annular reduction for the therapy of hear failure-induced mitral regurgitation. Circulation. 2003; 108:1795–1797. [PubMed: 14530194]

Kohn, R. Heart and cardiovascular system. Nostrand Reinhold; New York: 1977.

Laurent S, Boutouyrie P, Lacolley P. Structural and Genetic Bases of Arterial Stiffness. Hypertension. 2005; 45:1050–1055. [PubMed: 15851625]

Liddicoat JR, Mac Neill BD, Gillinov AM, Cohn WE, Chin CH, Prado AD, Pandian NG, Oesterle SN. Percutaneous Mitral Valve Repair: A Feasibility Study in an Ovine Model of Acute Ischemic Mitral Regurgitation. Catheterization and Cardiovascular Interventions. 2003; 60:410–416. [PubMed: 14571496]

Loukas M, Bilinsky S, Bilinsky E, El-Sedfy A, Anderson RH. Cardiac Veins: A Review of the Literature. Clinical Anatomy. 2009; 22:129–145. [PubMed: 19097063]

Maniu C, Patel JB, Reuter DG, Meyer DM, Edwards WD, Rihal CS, Redfield MM. Acute and Chronic Reduction of Functional Mitral Regurgitation in Experimental Heart Failure by Percutaneous Mitral Annuloplasty. Journal of the American College of Cardiology. 2004; 44:1652–1661. [PubMed: 15489099]

Pezet M, Mariko B, Jacob M, Faury G. The elastic fibres: A regulator of normal and pathological ageing of elastic blood vessels. Medecine et Longevite. 2009; 1:64–75.

Pham T, Sun W. Characterization of the mechanical properties of the coronary sinus for percutaneous transvenous mitral annuloplasty. Acta Biomaterialia. 2010 in press.

Sacks MS, Sun W. Multiaxial Mechanical Behavior of Biological Materials. Annu Rev Biomed Eng. 2003

Schulze-Bauer CAJ, Morth C, Holzapfel GA. Passive Biaxial Mechanical Response of Aged Human Iliac Arteries. Journal of Biomechanical Engineering. 2003; 125:395–406. [PubMed: 12929245]

Siminiak T, Firek L, Jerzykowska O, Katmucki P, Wotoszyn M, Smuszkiewicz P, Link R. Percutaneous valve repair for mitral regurgitation using the Carillon(TM)-Mitral Contour System(TM). Description of the method and case report. Kardiologia Polska. 2007; 65:272–278. [PubMed: 17436155]

Siminiak T, Hoppe UC, Schofer J, Haude M, Herrman JP, Vainer J, Firek L, Reuter DG, Goldberg SL, Bibber RV. Effectiveness and Safety of Percutaneous Coronary Sinus-Based Mitral Valve Repair in Patients With Dilated Cardiomyopathy (from the AMADEUS Trial). Am J Cardiology. 2009; 104:565–570.

Sun W, Sacks MS. Finite element implementation of a generalized Fung-elastic constitutive model for planar tissues. Biomechanics and Modeling in Mechanobiology. 2005; 4:190–199. [PubMed: 16075264]

Sun W, Sacks MS, Sellaro TL, Slaughter WS, Scott MJ. Biaxial Mechanical Response of Bioprosthetic Heart Valve Biomaterials to High In-plane Shear. Journal of Biomedical Engineering. 2003; 125:372–380.

Tritthart H, P. MD, Stierle HE, Krause H. Effects of Ca-Free and EDTA-Containing Tyrode Solution on Transmembrane Electrical Activity and Contraction in Guinea Pig Papillary Muscle. Pfliigers Arch. 1973; 338:361–-376.

Webb JG, Harnek J, Munt BI, Kimblad PO, Chandavimol M, Thompson CR, Mayo JR, Solem JO. Percutaneous transvenous mitral annuloplasty: initial human experience with device implantation in the coronary sinus. Circulation. 2006; 113:851–855. Epub 2006 Feb 2006. [PubMed: 16461812]
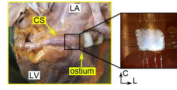
Figure 1.
The anatomy of the intact coronary sinus (**CS**) vessel showing the excised location for biaxial testing. The image on the right shows the CS specimen mounted in the biaxial machine bath. **C** - circumferential, **L** - longitudinal, **LA** - left atrium, **LV** - left ventricle.
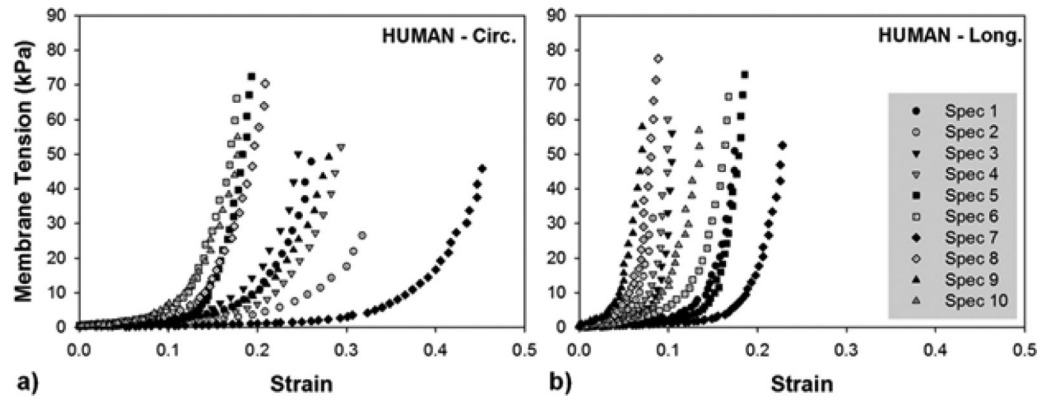
Figure 2.
Equibiaxial results of ten human coronary sinus specimens in a) the circumferential (**Circ.**) and b) longitudinal (**Long.**) directions.
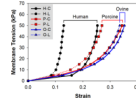
Figure 3.
Mean equibiaxial responses of human (**H**), porcine (**P**) and ovine (**O**) CS tissues in the circumferential (**C**) and longitudinal (**L**) directions.
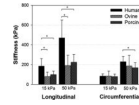
Figure 4.
Tissue stiffness computed at membrane tensions of 15 and 50 kPa, comparing between human, ovine, and porcine tissues. (*) indicates the statistical significant difference between the two pairs. Data are presented as mean and standard deviation.
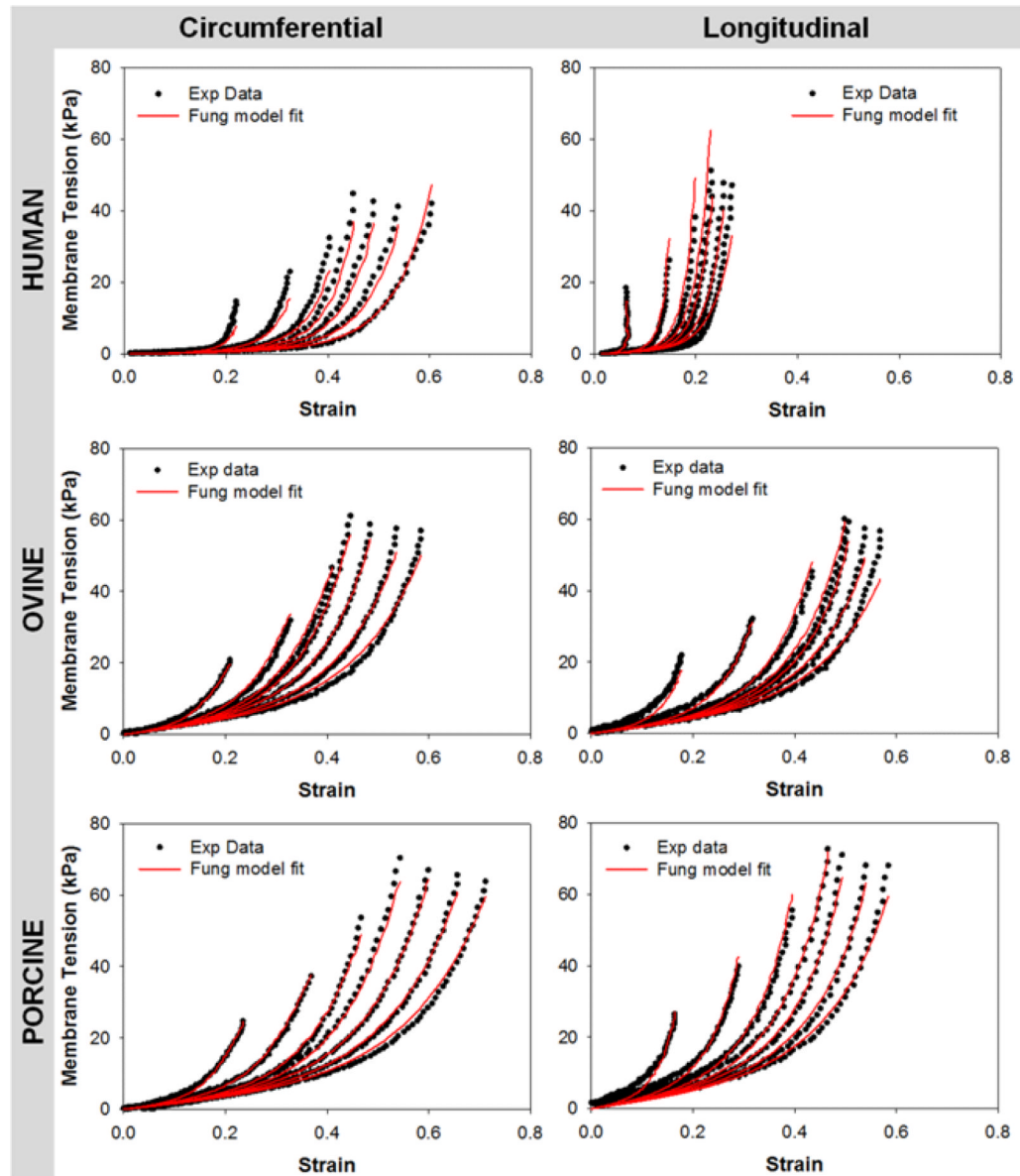
Figure 5.
Representative stress-strain response data for human (top row), ovine (middle row) and porcine (bottom row) CS tissues (dot lines) fitted with Fung elastic model (red lines). **CIRC** - circumferential direction, **LONG** – Longitudinal direction.
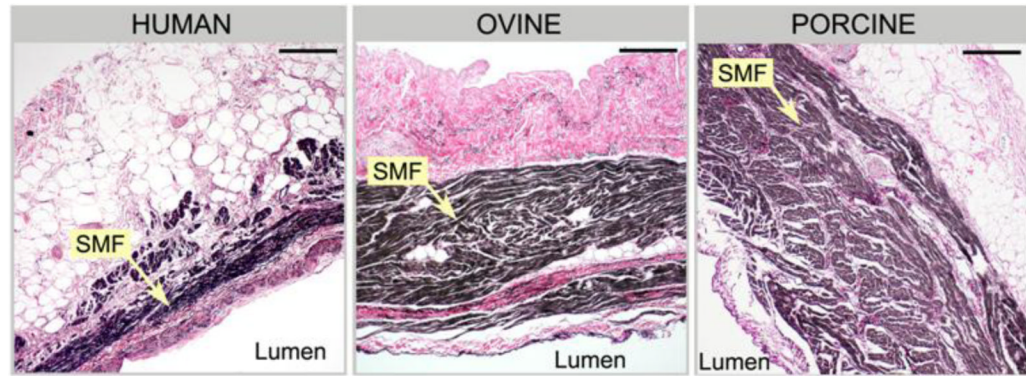
Figure 6.
The cross-section histological results of human, ovine, and porcine posterior CS sections in the circumferential direction. Human CS is thinner with less striated myocardial fibers (**SMF**) and exhibits a higher elastin/collagen contents than ovine and porcine CS in the intima layer. Black fibers - elastin, pink fibers - collagen, brown fibers - striated myocardial fibers. (x100 Magnification, bar length is 200 μm).
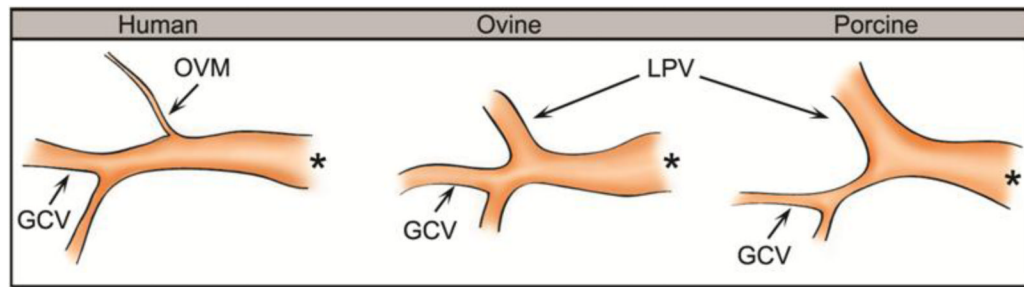
Figure 7.
A sketch of the tributaries of the coronary sinus vessel, showing the tapered oblique vein of Marshall (**OVM**) in human and the patent left precaval vein (**LPV**) in ovine and porcine tissues. The great cardiac vein (**GCV**) of porcine is narrowest among the three species. (*) indicates the ostium of the CS vessel.

Table 1

Anamnesis of patients

					Specimens						
	1	2	3	4	5	6	7	8	9	10	Mean ± SD
Age (yrs)	69	88	78	96	95	79	98	87	80	95	86.5 ± 9.70
Sex	M	F	M	F	F	F	F	F	F	M	-
PMR (hr)	22	11	10	21	7	11	18	8	21.5	23.7	15.32 ± 6.51
Cause of death	HB	Alz	CPA	CPA	RA	CPA	RA	Alz	ukn	NC	-
Primary disease	HB	CAD	CA	ukn	ukn	Hyp	ukn	ukn	PKD	n	-
Risk factors											
Hypertension	y	n	y	n	n	y	n	n	n	n	-
Cholesterol	n	n	n	n	n	n	n	n	n	n	-
Diabetes	y	ukn	n	n	n	ukn	y	n	n	n	-
GERD	n	y	n	n	n	n	n	n	n	n	-
Pneumonia	n	n	n	n	y	n	n	n	n	n	-
Dementia	n	n	n	n	n	n	n	y	n	n	-
Atherosclerosis											
Coronary	n	y	n	n	n	n	n	n	n	n	-

PMR = post-mortem recovery time, **Alzheimer's** = Alz, **CA** = cardiac arrest, **CAD** = Coronary artery disease, **CHF** = Chronic heart failure, **CPA** = Chronic pulmonary aspergillos, **COPD** = Chronic obstructive pulmonary disease, **GERD** = Gastroesophageal reflux disease, **HB** = Heart blockage, **Hyp** = Hypertension, **NC** = Natural causes (old age), **RA** = Respiratory arrest, **PKD** = Polycystic Kidney Disease, **ukn** = unknown.

Table 2

Fung model parameters for human, ovine and porcine CS specimen.

Specimen	C	A1	A2	A3	A4	A5	A6	R^2
Human	0.47 ± 0.28	28.62 ± 12.94	76.10 ± 30.76	1.99 ± 7.69	48.80 ± 16.52	-0.10 ± 4.08	-2.79 ± 8.66	0.95 ± 0.03
Ovine	6.22 ± 3.07	9.22 ± 8.77	12.28 ± 14.31	0.45 ± 3.86	10.82 ± 12.43	-0.25 ± 1.12	-0.24 ± 1.78	0.93 ± 0.05
Porcine	7.99 ± 10.17	4.17 ± 2.29	9.85 ± 6.45	1.59 ± 2.43	6.84 ± 2.97	-0.14 ± 0.56	0.20 ± 0.44	0.93 ± 0.09

Data are presented as mean ± standard deviation.